



# Heterogeneous shear elasticity of glasses: the origin of the boson peak

Alessia Marruzzo<sup>1,2</sup>, Walter Schirmacher<sup>1,3</sup>, Andrea Fratallocchi<sup>2</sup> & Giancarlo Ruocco<sup>1</sup>

<sup>1</sup>Dipartimento di Fisica, Università di Roma "La Sapienza", P.le Aldo Moro 2, I-00185, Roma, Italy, <sup>2</sup>PRIMALIGHT, Faculty of Elect. Engineering; Applied Mathematics and Computational Science, King Abdullah University of Science and Technology (KAUST), Thuwal 23955-6900, Saudi Arabia, <sup>3</sup>Institut für Physik, Universität Mainz, Staudinger Weg 7, D-55099 Mainz, Germany.

SUBJECT AREAS:  
CONDENSED-MATTER  
PHYSICS  
PHYSICS  
NANOSCIENCE AND  
TECHNOLOGY  
NANOSCALE MATERIALS

Received  
19 December 2012

Accepted  
19 February 2013

Published  
8 March 2013

Correspondence and  
requests for materials  
should be addressed to  
A.F. (andrea.  
fratallocchi@kaust.edu.  
sa)

The local elasticity of glasses is known to be inhomogeneous on a microscopic scale compared to that of crystalline materials. Their vibrational spectrum strongly deviates from that expected from Debye's elasticity theory: The density of states deviates from Debye's law, the sound velocity shows a negative dispersion in the boson-peak frequency regime and there is a strong increase of the sound attenuation near the boson-peak frequency. By comparing a mean-field theory of shear-elastic heterogeneity with a large-scale simulation of a soft-sphere glass we demonstrate that the observed anomalies in glasses are caused by elastic heterogeneity. By observing that the macroscopic bulk modulus is frequency independent we show that the boson-peak-related vibrational anomalies are predominantly due to the spatially fluctuating microscopic shear stresses. It is demonstrated that the boson-peak arises from the steep increase of the sound attenuation at a frequency which marks the transition from wave-like excitations to disorder-dominated ones.

The high-frequency vibrational dynamics of glasses (in the regime of a few THz or meV) is in the focus of experimental, theoretical and computational work for already half a century<sup>1,2</sup>. Whereas the crystalline-lattice dynamics is well understood in terms of the symmetry-related phonon dispersions, supplemented by the consideration of phonon-phonon interactions<sup>3</sup>, the theoretical interpretation of vibrational spectra of glasses, which differ considerably from those of crystals, is a matter of fierce controversies. The anomalous features are (i) an enhancement of the density of states  $g(\omega)$  over Debye's  $g(\omega) \propto \omega^2$  law in a regime, where elasticity theory should still hold, i.e. 1/10 of a Debye frequency, ("boson peak", BP)<sup>3,4</sup>, please see Ref.2 for further references]; (ii) a frequency dependence of the sound attenuation (width of the Brillouin line) which shows a strong increase near the BP frequency; (iii) a negative dispersion of the sound velocities followed by a characteristic minimum near the BP frequency<sup>5-8</sup>.

These features can be related to anomalies in the temperature dependence of the specific heat  $C(T)$ <sup>9</sup> and the thermal conductivity  $\kappa(T)$ <sup>10</sup>. The former - if plotted as  $C(T)/T^3$  shows a peak near  $\sim 10$  K, which is also called boson peak, and the latter shows a characteristic shoulder at the BP temperature, which has been shown to be essentially an "upside-down" BP<sup>11</sup>. The Raman spectra of glasses show also an anomalous maximum near the BP frequency (which is also called boson peak). Its relation to the other vibrational anomalies has been discussed recently<sup>12-14</sup>.

Models for the BP and the associated anomalies<sup>15</sup> range from assuming quasi-local vibrational states, produced by soft anharmonic potentials<sup>16-18</sup> over elastic heterogeneities<sup>11,19-23</sup> to broadened and shifted van-Hove-singularities<sup>24,25</sup>.

However, a number of recent inelastic scattering experiments<sup>5-8,26,27</sup> and molecular-dynamics (MD) simulations<sup>28-36</sup> gave valuable insights into the nature of the high-frequency and small-scale vibrational properties of glasses. It emerges that the disorder-affected transverse degrees of freedom of local elasticity play a key role for producing the anomalies.

By analyzing the acoustical properties of 2- and 3-dimensional model glass systems it was found<sup>29,34,35</sup> that the BP frequency corresponds to the transverse Ioffe-Regel (IR) frequency, i.e. the frequency at which the wavelength of a transverse excitation is equal to its mean-free path. Such a coincidence of the BP frequency with the transverse IR frequency is found also in our data to be presented below. In metallic glasses<sup>37</sup> the BP position also coincides with the transverse Ioffe-Regel frequency, whereas in a number of other glasses coincidence with the longitudinal IR frequency is found<sup>38</sup>. By a fundamental principle of wave mechanics this implies that vibrational states with frequencies above the BP frequency cannot be labelled with a wave vector  $k$ . Therefore, above the Ioffe-Regel



frequency, there is no reason for the existence of a Debye law. This is - in a nutshell - already the explanation of the BP phenomenon.

As a matter of fact, such a scenario appears quite naturally if one assumes that the local elastic moduli fluctuate from location to location in space (elastic heterogeneity)<sup>11,23</sup>. The existence of elastic heterogeneities in glasses have been postulated already for a long time<sup>39–41</sup>. There exists by now both experimental<sup>12,43</sup> as well as simulational<sup>33,36,44–46</sup> evidence - including the data to be presented below - for the existence of elastic heterogeneity in glasses. The computational data reveal that, in fact, the shear-elastic fluctuations are dominant.

Most of the papers dealing with the BP and the other vibrational anomalies of glasses start with the sentence “Although much scientific work has been done on the vibrational anomalies the origin of the boson peak remains elusive” or so. This is in spite of a large body of investigations, which show that the anomalies are related to (and caused by) the structural disorder of the glassy materials<sup>1,2,11,15–23,28,30–36</sup>.

In the present contribution we show by comparing a simulation of a very large soft-sphere glassy system with the heterogeneous-elasticity theory<sup>11,23</sup> that the spatial fluctuations of the elastic constants on a microscopic length scale produce the boson peak and the other elastic anomalies. By evaluating the eigenvalues of the Born-Kelvin stiffness matrix within the simulation we verify for the first time quantitatively the correctness of the model assumptions of the theory. The theory is also shown to account for the non-affine character of disordered shear elasticity<sup>31,32</sup>. We further demonstrate that the vibrational anomalies are mainly due to the fluctuations of the

shear stresses. This is achieved by investigating the frequency dependence of the macroscopic elastic moduli.

## Results

**Vibrational spectra of a soft-sphere glass.** In order to extract the vibrational properties of our model glass we have calculated the longitudinal ( $L$ ) and transverse ( $T$ ) current-current correlation functions  $C_{L,T}(k, \omega)$  as well as the vibrational density of states (DOS)  $g(\omega)$ , obtained via the local velocity autocorrelation functions<sup>47</sup>. In Fig. 1 we show examples for  $C_{L,T}(k, \omega)$  data.

The  $C_{L,T}(k, \omega)$  data could well be fitted by a damped-harmonic oscillator function (DHO)

$$\begin{aligned} C_{L,T}(k, \omega) &\propto \omega \operatorname{Im} \left\{ \frac{1}{\Omega_{L,T}^2(k) - \omega^2 - i\omega\Gamma_{L,T}(k)} \right\} \\ &= \frac{\omega}{k^2} \operatorname{Im} \{ \chi_{L,T}(k, \omega) \} \\ &= \omega^2 \frac{\Gamma_{L,T}(k)}{(\Omega_{L,T}(k)^2 - \omega^2)^2 + \omega^2 \Gamma_{L,T}(k)^2}, \end{aligned} \quad (1)$$

where we have introduced the longitudinal and transverse Brillouin resonance frequencies  $\Omega_{L,T}(k)$ , the corresponding Brillouin line widths  $\Gamma_{L,T}(k)$  (sound attenuation coefficients) and the complex longitudinal and transverse dynamic susceptibilities  $\chi_{L,T}(k, \omega)$ . The resonance frequencies  $\Omega_{L,T}$  turned out to be essentially linear in the investigated regime ( $k_{\min} = 0.031 \leq k \leq k_{\max} = 1.426$ ), i.e.  $\Omega_{L,T} = v_{L,T}k$ . Therefore we find it appropriate to represent the data - as in optics - in terms of *complex, frequency-dependent sound velocities*:

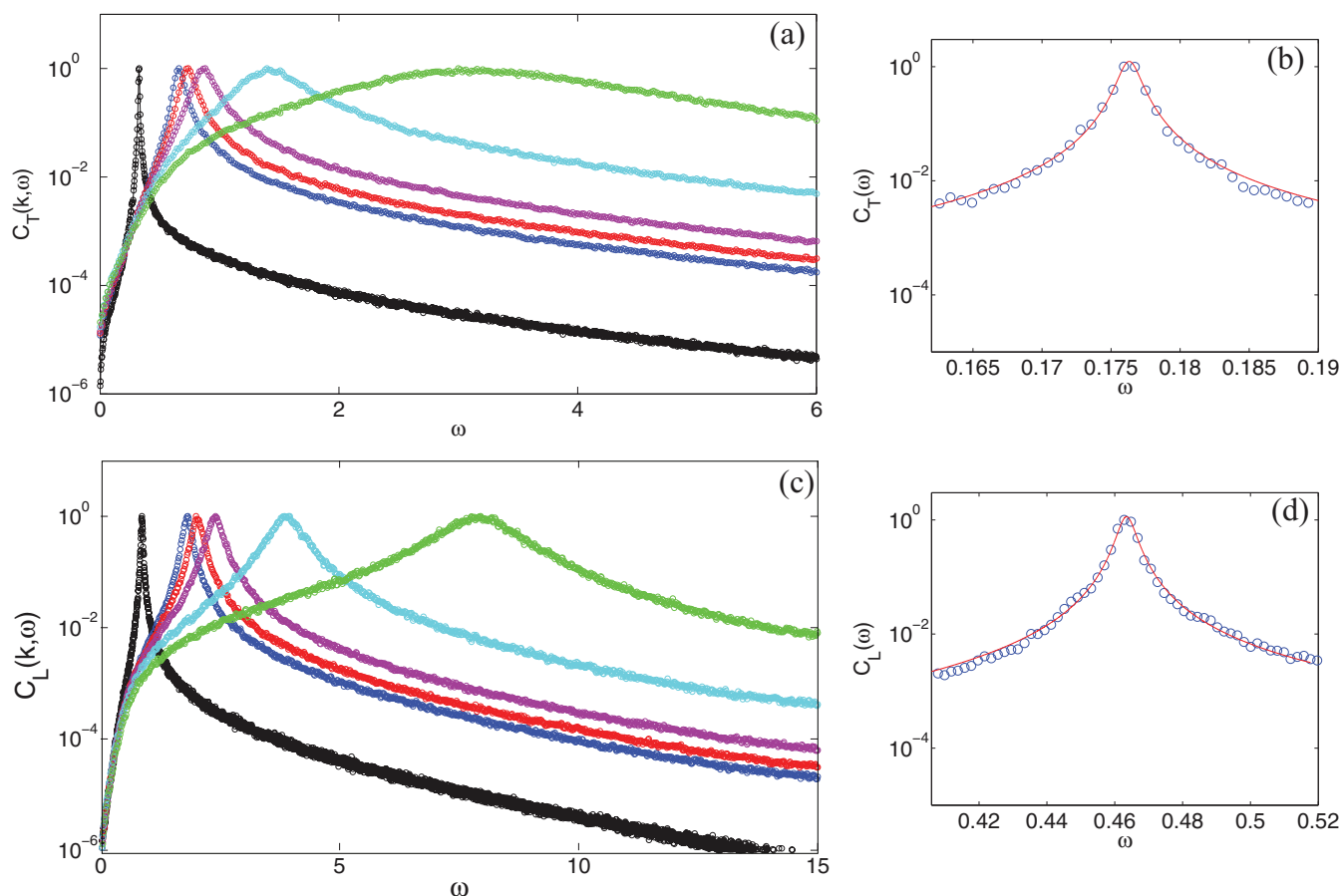


**Figure 1** | Longitudinal (a–b) and transverse (c–d) current-current correlation functions  $C_{L,T}$  for  $k = 0.14, 0.30, 0.33, 0.39, 0.63, 1.2$  (LJ units). In the panels b and d, we provided an example of the fit with the DHO function given by Eq. (1) for  $k = 0.076$  (solid line). Fit data are  $\Omega_T = 0.176$ ,  $\Omega_L = 0.464$ ,  $\Gamma_T = 1.5 \cdot 10^{-3}$ ,  $\Gamma_L = 5.4 \cdot 10^{-3}$ .



$$\chi_{L,T} = \frac{k^2}{-\omega^2 + k^2 \hat{v}_{L,T}(\Omega_{L,T}, \omega)^2} \quad (2a)$$

$$v_{L,T}^2(\Omega_{L,T}, \omega) = \frac{1}{k^2} [\Omega_{L,T}(k)^2 - i\omega \Gamma_{L,T}(k)] \quad (2b)$$

$$\approx v_{L,T}'(\omega)^2 [1 - i\Gamma_{L,T}(\omega)/\omega] \Big|_{\omega=\Omega_{L,T}(k)} \quad (2c)$$

$$\equiv \hat{v}_{L,T}(\omega)^2 \Big|_{\omega=\Omega_{L,T}(k)} \quad (2d)$$

The real parts  $v_{L,T}'(\omega)$  of the complex sound velocities represents the apparent sound velocities in the low-frequency regime, their imaginary parts are related to the sound attenuation. It is worthwhile remarking that the approximation leading to Eq. (2c) is valid for  $\Gamma_{L,T}/\Omega_{L,T} \ll 1$ . As can be seen from Fig. 2 this ratio does not exceed  $\approx 0.15$  for the longitudinal and  $\approx 0.3$  for the transverse case.

In the low-frequency regime one can calculate from the complex sound velocities  $\hat{v}_{L,T}(\omega) = v_{L,T}'(\omega) - i v_{L,T}''(\omega)$  frequency-dependent wavelengths  $\lambda$  and mean-free paths  $\ell$  of the longitudinal and transverse wave-like excitations as  $\lambda_{L,T}(\omega)^{-1} = \omega/2\pi \text{Re}\{1/\hat{v}_{L,T}\} \approx \omega/2\pi v_{L,T}'(\omega)$  and  $\ell_{L,T}(\omega)^{-1} = \omega \text{Im}\{1/\hat{v}_{L,T}\} \approx \Gamma_{L,T}/2v_{L,T}'$ . When these lengths are equal to each other, the Ioffe-Regel regime  $\Omega = \pi\Gamma$  is reached. Near and beyond this regime the vibrational excitations are no more wave-like, and  $k$  cannot be used for labeling the vibrational excitations.

In the inset of Fig. 2 the reduced density of states  $g(\omega)/\omega^2$  is shown for the three temperatures considered (see Fig. 2 and “Methods”). The reduced DOS shows the BP anomaly typical for glasses. From Fig. 2 we see that the Ioffe-Regel limit is reached for the transverse waves near  $\Omega_T \approx 1$ , which is roughly the BP frequency, i.e. the frequency, where the density of states  $g(\omega)$  is no more Debye-like. This is understood easily if one realizes that  $g(\omega)$  is essentially given by the  $k$  sum of the combination  $C_L(k, \omega) + 2C_T(k, \omega)$  (see Eq. (8) below). As the weighting factors are the inverse cubes of the sound velocities the spectrum is dominated by the transverse part. For small  $k$  where  $\ell$  is much larger than  $\lambda$ ,  $C_{L,T}(k, \omega)$  are proportional to

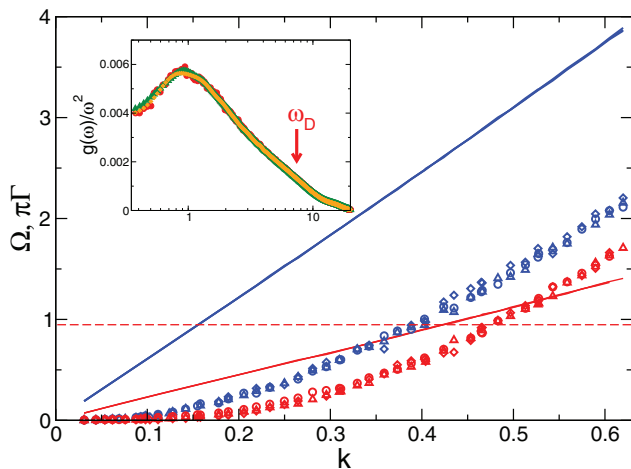


**Figure 2** | Resonance frequencies  $\Omega_{L,T}(k)$  (straight lines) and Brillouin line widths  $\Gamma_{L,T}(k)$ , multiplied with  $\pi$  for three temperatures  $T_1 = 5 \cdot 10^{-5}$  (circles),  $T_2 = 5 \cdot 10^{-4}$  (triangles),  $T_3 = 5 \cdot 10^{-3}$  (diamonds). Upper (blue) curves: longitudinal, lower (red) curves: transverse. The three curves for  $\Omega_{L,T}(k)$  lie on top of each other. The dashed line indicates the BP position, which is near the transverse Ioffe-Regel crossing. Insert: Reduced density of states  $g(\omega)/\omega^2$  as obtained from the velocity autocorrelation function for the three temperatures  $T_1$  (red circles),  $T_2$  (green triangles),  $T_3$  (orange diamonds). The arrow indicates the Debye frequency  $\omega_D = 7.54$  in LJ units.

$\delta(\omega - \Omega_{L,T})$ , which gives a Debye spectrum. Near the Ioffe-Regel limit  $C_T(k, \omega)$  deviates strongly from a sharply peaked function, which explains the non-Debye behavior: The BP is due to the breakdown of homogeneous elasticity in the transverse channel.

In Fig. 3 we have plotted the sound velocities  $v_{L,T}'$  and the Brillouin line widths  $\Gamma_{L,T}$  as a function of frequency. It is very striking that the velocities have a characteristic minimum near the frequency  $\omega \approx 1$  (in Lennard-Jones LJ units, see “Methods”), where the reduced DOS has its maximum (boson peak). These findings are similar to those found experimentally<sup>5,6</sup> and by simulation<sup>35</sup> previously. Below the BP frequency there is a strong increase of the line widths with increasing frequency, which, in the transverse case, is almost as strong as Rayleigh’s  $\omega^4$  law. Above the BP frequency the frequency dependence is much weaker. In the longitudinal case there is also a rapid increase of the attenuation below the BP frequency, but not as strong as  $\omega^4$ .

How does the strong frequency dependence, which leads to the breakdown of Debye elasticity at the BP frequency, come about? It is well known since the time of Lord Rayleigh<sup>48,49</sup> that inhomogeneities in a medium, which supports waves, lead to elastic scattering of the Rayleigh type, i.e.  $\ell^{-1} \propto \omega^{4.5-5.3}$ . In glasses at low frequencies this disorder-induced frequency dependency can be masked by anharmonic damping phenomena. However, there is now experimental<sup>5,6</sup> and numerical evidence<sup>34</sup> [and Fig. 3d] for the existence of the Rayleigh scattering mechanism in glasses between the anharmonic regime and the BP.

Using the complex sound velocities we now introduce complex macroscopic elastic moduli, namely the shear modulus  $G = \rho \tilde{G} = \rho \hat{v}_T^2$ , the longitudinal modulus  $M = \rho \tilde{M} = \rho \hat{v}_L^2$  and the bulk modulus  $K = \rho \tilde{K} = M - (4/3)G$  ( $\rho$  is the mass density).

Let us now discuss the frequency dependence of the moduli, displayed in Fig. 4. If we do the subtraction  $\tilde{M}(\omega) - (4/3)\tilde{G}(\omega) \equiv \tilde{K}(\omega)$  it turns out that the real part of  $\tilde{K}$  is frequency independent and its imaginary part is almost zero. It can be seen clearly from Fig. 4 that the real and imaginary part of the quantity  $(4/3)(\tilde{G}(\omega) + \tilde{K})$ , where  $\tilde{K} = 30.4$  is the frequency-independent reduced bulk modulus, exhibits the same frequency dependence as those of the complex longitudinal modulus  $\tilde{M}(\omega)$ . The observation that the macroscopic bulk modulus is frequency independent, as we shall argue below, points to the fact that the vibrational anomalies in our model glass are predominantly due to spatially fluctuating shear stiffnesses. A frequency-independent bulk modulus has been found recently in a

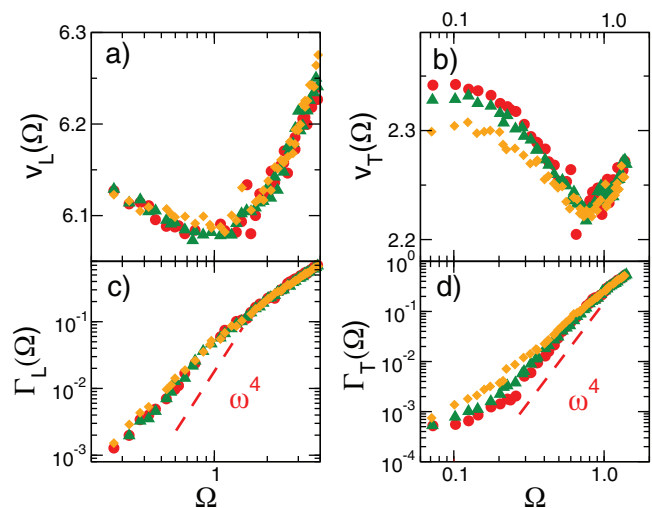


**Figure 3** | Frequency dependence of the longitudinal and transverse sound velocities (a) and (b) and corresponding sound attenuation coefficients (c) and (d), as extracted from the current-current autocorrelation functions using the damped-harmonic-oscillator parametrization, Eq. (1) for the three temperatures specified in Fig. 2.

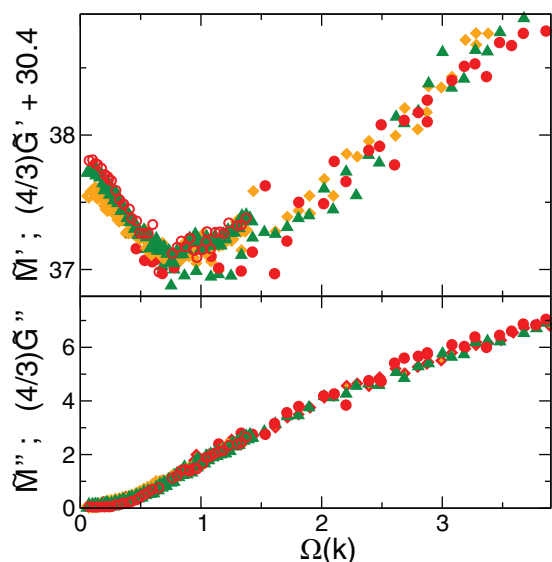


**Figure 4** | Frequency dependence of the real parts (top) and imaginary parts (bottom) of the elastic moduli:  $\tilde{M}(\Omega_L)$  (full symbols) and  $4/3\tilde{G}(\Omega_T) + \tilde{K}'$  (open symbols) with  $\tilde{K}' \equiv \text{Re}\{\tilde{K}\} = 30.4$  for the three temperatures specified in Fig. 2. The imaginary part of  $\tilde{K}$  turned out to be zero in all cases.

simulation of a LJ glass<sup>35</sup> pointing to the conclusion that quite generally in central-potential glasses the BP producing elastic heterogeneities are dominated by the shear degrees of freedom.

**Heterogeneous-elasticity theory.** Let us now discuss these findings in terms of heterogeneous-elasticity theory<sup>11,23</sup>. The equation of motion for a Cartesian component of a local displacement vector  $\mathbf{u}(\mathbf{r}, \omega)$  can be written in terms of the stress tensor  $\sigma_{ij}$  (where  $i, j = 1, 2, 3$  are the Cartesian indices) as

$$-\omega^2 \rho u_i(\mathbf{r}, \omega) = \sum_j \partial_j \sigma_{ij} \quad (3)$$

with  $\partial_j \equiv \partial/\partial x_j$ . Hooke's law, which relates  $\sigma_{ij}$  to the strain tensor  $\epsilon_{ij} = 1/2(\partial_i u_j + \partial_j u_i)$  in an isotropic system can be written in two different ways:

$$\sigma_{ij} = \left( K - \frac{2}{3}G \right) \delta_{ij} \text{Tr}\{\epsilon\} + 2G\epsilon_{ij} \quad (4a)$$

$$= K\delta_{ij} \text{Tr}\{\epsilon\} + 2G\hat{\epsilon}_{ij} \quad (4b)$$

where we have introduced the trace-free strain tensor

$$\hat{\epsilon}_{ij} = \epsilon_{ij} - \frac{1}{3} \delta_{ij} \text{Tr}\{\epsilon\} \quad (5)$$

The representation (4b) implies a separation between pure dilatational and pure shear stresses. The quantity  $\hat{\sigma}_{ij} = 2G\hat{\epsilon}_{ij}$  is the traceless tensor of dilatational-free stresses. On a small scale the elastic constants  $K$  and  $G$  may depend on the spatial location  $\mathbf{r}$ , which is the definition of elastic heterogeneity. The assumption of spatial statistical fluctuations of the shear modulus according to a Gaussian distribution with mean  $G_0$  and variance  $\langle \Delta G^2 \rangle$  is the basis of heterogeneous-elasticity theory<sup>11,23</sup>.

On a large scale the spatial fluctuations transform into a frequency dependence including a real and imaginary part. Within the Ioffe-Regel regime (Debye regime) this frequency dependence of the large-scale complex elastic moduli are induced by scattering from the elastic inhomogeneities. Due to the macroscopic homogeneity of the system the microscopic inhomogeneities of the stress tensor are mapped to a frequency dependence of the macroscopic stresses.

In the original formulation of the theory<sup>11,23</sup> the first term in Eq. (4a) (Lamé's  $\lambda$  parameter) was assumed not to fluctuate spatially which leads to a frequency-dependent macroscopic bulk modulus. As such a frequency dependence is not observed, our conclusion is that in glasses with frequency-independent bulk modulus *the BP-related vibrational anomalies are entirely produced by shear stresses*. The present version of our theory is therefore formulated in such a way that the shear modulus  $G$  that appears in the second term of Eq. (4b) fluctuates with a Gaussian distribution of the deviation  $\Delta G$  from the mean  $G_0$ , i.e. the bulk modulus  $K$  is not assumed to fluctuate.

It is very important to emphasize that the disorder-induced frequency dependence of the elastic moduli  $M$  and  $G$  has nothing to do with dissipation. In a disordered harmonic solid there is no damping. The apparent frequency dependence is due to the fact that with increasing frequency the concepts of macroscopic elasticity theory, namely the labeling of the vibrational states by wavenumbers breaks gradually down, until it becomes entirely meaningless at the Ioffe-Regel limit. This is the reason, why crystalline concepts like van-Hove singularities<sup>24,25</sup>, which rely on well-defined dispersion relations (with no imaginary part involved), are not very helpful in discussing the vibrational states of a glass.

The mean-field theory for heterogeneous shear elasticity gives the following self-consistent equations for the macroscopic moduli (self-consistent Born approximation, SCBA):

$$\tilde{G}(\omega) = \tilde{G}_0 - \Sigma(\omega) = \hat{v}_T^2(\omega) \quad (6a)$$

$$\tilde{M}(\omega) = \tilde{K} + \frac{4}{3}\tilde{G}(\omega) = \hat{v}_L^2(\omega) \quad (6b)$$

$$\Sigma(\omega) = \gamma \tilde{G}_0^2 \frac{1}{N} \sum_{|k| < k_D} \left[ \frac{2}{3} \chi_L(k, \omega) + \chi_T(k, \omega) \right] \quad (6c)$$

with  $\chi_{L,T}(k, \omega)$  given by Eq. (2a). The influence of the disorder is given by the complex self-energy function  $\Sigma(\omega)$ . The  $\mathbf{k}$  summation  $\frac{1}{N} \sum_{|k| < k_D} \equiv \frac{3}{k_D^3} \int_0^{k_D} k^2 dk$  is restricted to values smaller than the Debye wavenumber  $k_D = \sqrt[3]{6\pi^2 N/V}$ .  $N$  is the number of atoms and  $V$  is the volume of the sample.

$$\gamma = (N/V) V_c \langle \Delta G^2 \rangle / G_0^2 \quad (7)$$

is the disorder parameter, where  $V_c$  is the coarse-graining volume used to calculate the local shear modulus  $G$ . The second parameter of the theory is the ratio  $K/G_0$ . The density of states is given by

$$g(\omega) = \frac{2\omega}{3\pi} \text{Im} \left\{ \frac{1}{N} \sum_{|k| < k_D} \frac{1}{k^2} [\chi_L(k, \omega) + 2\chi_T(k, \omega)] \right\} \quad (8)$$

Due to the assumption of a Gaussian distribution of microscopic shear fluctuations there exists a critical value of the disorder parameter  $\gamma_c$  beyond which the system is unstable. The instability arises because of the presence of negative shear stiffnesses. (As a matter of fact, there is evidence from numerical work on metallic glasses<sup>33,40</sup> for the existence of Gaussian distributions of local shear stiffnesses, which extend to negative values.)  $\gamma_c$  depends weakly on the ratio  $K/G_0$  and is of the order of 0.2. As noted already earlier<sup>11,20,23</sup> the vibrational anomalies can be interpreted as precursor phenomena of the instability, which occurs at lower density or higher temperature<sup>54</sup>.

In Fig. 5 the real and imaginary parts of  $\tilde{G}$  are compared to the result of the theory with  $\gamma_c - \gamma = 0.008$ , and  $K/G_0 = 3.166$ . In Fig. 6 the reduced DOS of the simulation is compared with the prediction of the theory for the same parameters. The agreement is striking! At very low frequencies, where the data are temperature dependent and deviate from the Rayleigh law, anharmonic physics becomes distinct. We shall discuss this frequency regime in a forthcoming paper.

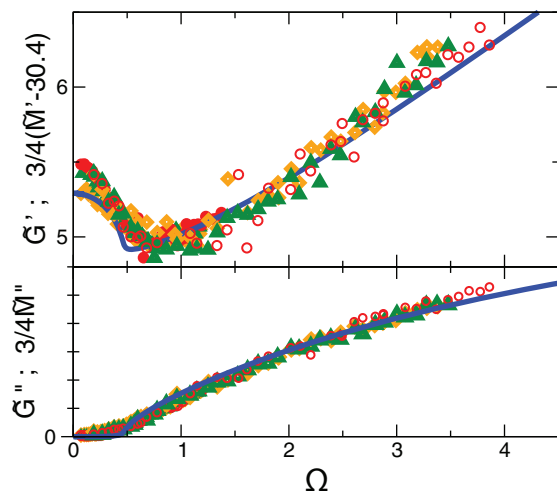


**Figure 5** | Real parts (upper panel) and imaginary parts (lower panel) of the frequency-dependent shear modulus  $\tilde{G}(\Omega_T)$  and the quantity  $3/4(\tilde{M}(\Omega_L) - \tilde{K})$  for all three temperatures with  $\tilde{K} = 30.4$ . Symbols: simulation data for all three temperatures (same code as in Fig. 3). Full line: SCBA calculation of  $\tilde{G}(\omega)$  (which equals  $3/4(\tilde{M}(\omega) - \tilde{K})$ ) with  $\gamma_c - \gamma = 0.008$  and  $K/G_0 = 3.166$ .

**Local elasticity fluctuations.** In order to further test the reliability of the theory we have calculated the local 6 eigenvalues  $C_1 \dots C_6$  of the matrix of the Born-Kelvin stiffness coefficients (see “Methods”) for different coarse-graining volumes  $V_c$ . In an isotropic system  $C_1 = 3K$  and  $C_i = 2G$ ,  $i \geq 2$ . The results are displayed in Fig. 7. In the main body of the figure the distribution of the  $C_i$  are shown for  $V_c = 45$  and  $V_c = 2000$  (the total volume is  $V = 8.3 \cdot 10^6$  in LJ units). In the insert the mean values and  $\gamma$  parameters, defined as in Eq. (7) are plotted against  $V_c$ . The value of  $\langle C_1 \rangle \approx 100$  for large  $V_c$  essentially agrees with the value  $3K = 3\rho\tilde{K} = 109$  ( $\rho = 1.2$  in LJ units) extracted from the frequency-dependent moduli (Fig. 4). The mean values of the shear eigenvalues are  $\approx 33$ , giving  $\langle G \rangle \approx 16$ . This nicely corresponds to  $G_0/K \approx 3$  used in our fits. However  $\langle G \rangle$  does *not* agree to the macroscopic value of  $G = \rho v_T^2 \approx 6.5$  (Figs. 3, 5). The reason is that the Born expressions for the stiffness coefficients  $C_{ij}$  rely on the assumption of affinity of the dilatational and shear elasticity of the solids.

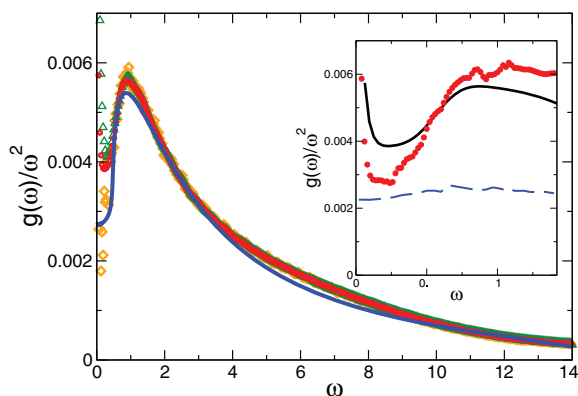


**Figure 6** | Reduced density of states. Symbols: simulation data as obtained from the velocity autocorrelation function for all three temperatures. Full line: Theory with the same value of  $\gamma$  as in Fig. 5. Insert: reduced density of states for the lowest temperature (full line), compared with the approximate reduced density of states calculated from the fit parameters  $c'_{L,T}(\omega)$  and  $\Gamma_{L,T}(\omega)$  of the simulated current-correlation functions using Eq. (9) (red dots). The dashed blue line is the Debye contribution corresponding to the first summand in Eq. (9).

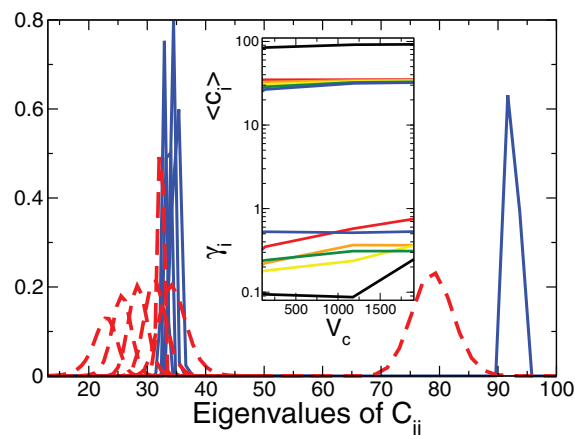


**Figure 7** | Histogram of the 6 eigenvalues  $C_{ij}$  of the Kelvin stiffness tensor  $C_{ij}$  evaluated using Born’s force constants for a tiling of the total volume into  $57^3$  boxes ( $V_c = 44$ , red dashes) and into  $16^3$  boxes ( $V_c = 2000$ , blue lines). The total volume is  $V = 8.3 \cdot 10^6$ . Insert: Mean values  $\langle C_i \rangle$  (top group) and disorder parameters  $\gamma_i = V_c(N/V)\langle \Delta c_i^2 \rangle / \langle c_i \rangle^2$  (bottom group) vs. coarse-graining volume  $V_c$ . The top and bottom black lines correspond to  $C_1 \xrightarrow{V_c \rightarrow \infty} 3K$ , the others to  $C_2 \dots C_6 \xrightarrow{V_c \rightarrow \infty} 2G$ .

As demonstrated in detail in a series of simulations<sup>31,32</sup>, this assumption does not hold for shear elasticity in glasses; the shear modulus is lowered by the presence of non-affine processes as compared to the Born expectation. This reduction of  $G$  is included in the predictions of our theory and is induced by the  $\omega = 0$  value of the self energy  $\Sigma$ . For  $\gamma \approx \gamma_c$  we have  $\Sigma(0) \approx 0.5G_0$ , which gives a reduction of a factor 0.5 in agreement with the simulation. As the function  $\Sigma(\omega)$  describes the BP-related vibrational anomalies, we can state that the appearance of the boson peak and the reduction of the shear modulus by the non-affine processes are both due to the elastic heterogeneities, viz. the structural disorder.

From Fig. 7 we see that all distributions of the  $C_i$  are Gaussian and that the  $\gamma$  value of  $C_1$  is much lower than those of the shear moduli. The latter are of the order or somewhat larger than  $\gamma_c \approx 0.2$ . We see that the model assumptions and parameters of our theory are quite realistic. We also see that on the microscopic scale spatial fluctuations of the compression modulus exist, but the *relative* fluctuations, represented by the  $\gamma$  value, are much smaller. This corresponds to similar findings in Refs. 31, 32. If the fluctuations of  $K$  would be stronger this would lead to a frequency-dependent  $K(\omega)$  and a further modification of the DOS in the BP regime. It is remarkable that also in the disorder-induced sound attenuation via tunneling systems the transverse degrees of freedom appear to be dominant, see e.g., G. Belessa, J. Phys. (Paris) **41**, C8-723 (1980); J. F. Berret and M. Meissner, Z. Phys. B - Condensed Matter **70**, 65 (1988).

## Discussion

We have argued that beyond the Ioffe-Regel limit, i.e. beyond the BP frequency there is no reason, why  $g(\omega)$  should exhibit a Debye law. But why is the disordered  $g(\omega)$  *larger* than the Debye density of states? We can answer this question by using a decomposition of the integrands in Eq. (8) as follows<sup>23</sup>:

Within the Ioffe-Regel regime i.e. for  $\omega$  below the BP position we approximately replace the denominator of the response functions  $-\omega^2 + k^2 v'_{L,T}{}^2(1 - i\Gamma(\omega)/\omega)$  by  $(1 - i\Gamma(\omega)/\omega)(-\omega^2 + k^2 v'_{L,T}{}^2)$ . This leads to a reduced density of states of the form

$$\frac{g(\omega)}{\omega^2} \approx \frac{1}{k_D^3} \left( \frac{1}{v'_L 3(\omega)} + \frac{2}{v'_T 3(\omega)} \right) + \frac{2}{\pi k_D^2} \left( \frac{1}{v'_L 2(\omega) \omega^2 + \Gamma_L^2(\omega)} + \frac{2}{v'_T 2(\omega) \omega^2 + \Gamma_T^2(\omega)} \right) \quad (9)$$



Now we can take our fit functions  $v'_{L,T}(\omega)$  and  $\Gamma_{L,T}(\omega)$  as determined from the simulated current correlation spectra and insert them into the formula. The results (for the lowest temperature  $T_1$ ) are the red symbols in the insert of Fig. 6. The straight line is  $g(\omega)/\omega^2$  as obtained from the velocity-autocorrelation function. The blue dashed line is the Debye-like contribution given by the first summand of Eq. (9). The difference between the symbols and the dashed line is entirely due to the broadening of the Brillouin line. The proportionality of the excess DOS to the sound attenuation constant in the sound-like regime has been pointed out already in Ref. 23.

We can now draw an important conclusion from considering the insert in Fig. 6. Monaco and Mossa<sup>35</sup> have argued that the BP is produced by the minimum in the real part of the frequency-dependent sound velocities assuming a Debye law as given by the first term in our equation (9). But this term just gives the rather weak maximum of the dashed curve. As pointed out above, the BP, instead, arises from the steep increase of the sound attenuation. The dip in the real part of the sound velocity is just the faint echo of this increase due to the Kramers-Kronig relations between the real and imaginary parts of the moduli.

We would like to emphasize again that the vibrational spectrum beyond the BP frequency cannot be described by concepts borrowed from Debye's theory: The disorder is dominant in this regime. It has been shown previously that the vibrational states in this regime obey the statistics of random matrices<sup>20</sup>. The eigenvalues exhibit level repulsion<sup>24</sup>, i.e. there are no degeneracies. This absence of degeneracies can be traced to the microscopic breakdown of the translational and rotational symmetry. We conclude that the vibrational states near and above the BP are of random-matrix type<sup>55</sup>.

We also would like to comment on the vibrational anomalies of SiO<sub>2</sub> glass, a material very-well investigated both experimentally and by computer simulation (please see Ref. 8 for an extensive bibliography on SiO<sub>2</sub>). A recent inelastic X-ray study<sup>8</sup> reveals that the elastic anomalies of this material can be qualitatively but not quantitatively explained in terms of elastic-heterogeneity theory (as presented in refs. 11, 23 and presently). To be specific, the measured excess density of states exceeds that predicted by the theory. Therefore an additional mechanism contributing to the boson peak was invoked. On the other hand, in recent theoretical work<sup>56</sup> the present theory, which is based on the assumption of a Gaussian distribution of the fluctuating elastic constants, has been generalized to include non-Gaussian distributions. This is achieved by using an off-lattice version of the coherent-potential approximation (CPA), which has been derived in Ref. 56. We convinced ourselves that non-Gaussian distributions produce a much stronger excess of the density of states than Gaussian ones. In particular the enhancement of the density of states of SiO<sub>2</sub> can be accounted for by assuming a power-law distribution, which can be derived from interatomic forces varying exponentially with distance. So the strong elastic anomalies of network-forming glasses can be explained by non-Gaussian heterogeneous elasticity.

Let us summarize our findings. By comparing a simulation of a very large model of a soft-sphere glass with the mean-field theory of elastic heterogeneous shear fluctuations we have obtained compelling evidence that the excess of the density of states over the Debye prediction (boson peak), the negative dispersion of the sound velocities and the steep increase in the Brillouin line width in the boson-peak region are produced by spatial fluctuations of dilatation-free shear stresses. More generally this points to the conclusion that in glasses the boson peak and the associated anomalies are induced by spatial fluctuations of elastic constants induced by the structural disorder. The strong Rayleigh-like scattering from the local inhomogeneities causes the breakdown of a wave-like description in favor of random-matrix type vibrational states. A theory has been formulated, which satisfactorily describes all anomalous features, including

the frequency independence of the bulk modulus and the non-affine shear elasticity of glasses.

## Methods

We simulated a 20 : 80 binary mixture of  $N = 10^7$  particles  $A_x B_{1-x}$  with  $x = 0.2$ , interacting through a soft-sphere potential. By choosing such a mixture crystallization is avoided, when the system is supercooled<sup>57</sup>. The two types of particles,  $A$  and  $B$ , have same masses,  $m_A = m_B = 1$ , but different soft-sphere potential parameters for the  $AA$ ,  $AB$  and  $BB$  interactions. The interaction potential is (we use standard LJ units):

$$\phi(r_{ij}) = 4\epsilon_{\alpha\beta} \left(\frac{\sigma_{\alpha\beta}}{r_{ij}}\right)^{12} - 4\epsilon_{\alpha\beta} \left(\frac{\sigma_{\alpha\beta}}{r_c}\right)^{12} \left(13 - 12\frac{r_{ij}}{r_c}\right) \quad (10)$$

with  $\sigma_{AA} = 1$ ,  $\sigma_{AB} = \sigma_{BA} = 0.80$ ,  $\sigma_{BB} = 0.88$  and  $\epsilon_{AA} = 1$ ,  $\epsilon_{AB} = \epsilon_{BA} = 1.50$ ,  $\epsilon_{BB} = 0.50$ .  $r_{ij}$  is the distance between particles  $i, j$  of species  $\alpha$  and  $\beta$ , respectively. This parametrization defines the standard molecular-dynamics units. The soft-sphere potential is continuously cut-off at  $r_c = 1.1856$ . At this value, with a mass density of  $\rho = 1.2$ , it guarantees a sufficiently large interaction distance to observe the formation of a super-cooled liquid. We performed an extremely massively campaign (about 20M of single-cpu computational hours) of parallel molecular dynamic simulations using the recently developed Billions-Body Molecular Dynamics (BBMD) package, which was specifically designed for massively parallel studies of amorphous materials<sup>58</sup>. We considered three different temperatures (in the standard MD units)  $T_1 = 5 \cdot 10^{-3}$ ,  $T_2 = 5 \cdot 10^{-4}$ ,  $T_3 = 5 \cdot 10^{-5}$ , which are well below the glass transition temperature that is estimated to be  $T_g \sim 0.1$ . The glass is formed by a controlled canonical evolution, where an input body-cubic lattice configuration is initially heated up to  $T = 3$ , and then slowly cooled down with a temperature decreasing linearly with time. The duration of the heating phase was  $\Delta t_h = 20$  (i.e., 20000 time steps), while the cooling period had a length of  $\Delta t_c = 2420$  (i.e.,  $2.42 \cdot 10^6$  time steps). The temperature of the system was adjusted by velocity rescaling every 10 time units ( $10^4$  elementary time steps). The collective motions have been studied by the calculation of the correlation functions

$$C_{L,T}(k, \omega) = \int dt \langle \mathbf{j}_{L,T}(\mathbf{k}, t) \mathbf{j}_{L,T}^*(\mathbf{k}, t_0) \rangle e^{i\omega t} \quad (11)$$

of the longitudinal and transverse current density vectors  $\mathbf{j}_L(\mathbf{k}, t) = \hat{\mathbf{k}} \cdot \mathbf{j}(\mathbf{k}, t)$ ,  $\mathbf{j}_T(\mathbf{k}, t) = \mathbf{j}(\mathbf{k}, t) - \mathbf{j}_L(\mathbf{k}, t)$  with  $\mathbf{j}(\mathbf{k}, t) = N^{-\frac{1}{2}} \sum_{i=1}^N \mathbf{v}_i \exp i\mathbf{k} \cdot \mathbf{r}_i$  and  $\mathbf{r}_i$  and  $\mathbf{v}_i$  are particle position and velocity, respectively. The vibrational density of state  $g(\omega)$ , conversely, was calculated by evaluating the local velocity autocorrelation function<sup>47</sup> of an ensemble of 16000 different particles.

$$g(\omega) \propto Z(\omega) = \int dt \frac{1}{3} (\mathbf{v}(t+t_0) \cdot \mathbf{v}(t_0)) e^{i\omega t} \quad (12)$$

$g(\omega)$  has been normalized to unity.

The local Hookean stiffness coefficients defined by  $\sigma_{\alpha\beta} = \sum_{\gamma\delta} C_{\alpha\beta\gamma\delta} \epsilon_{\gamma\delta}$  have been evaluated using the Born formula<sup>59</sup>

$$C_{\alpha\beta\gamma\mu} = \sum_r \frac{r_{in}}{r} [x_\alpha x_\beta x_\gamma x_\mu \frac{1}{2r^2} \left( \phi(r)'' - \frac{1}{r} \phi(r)' \right) + \frac{1}{8r} \phi(r)' (\delta_{\beta\mu} x_\alpha x_\gamma + \delta_{\alpha\mu} x_\beta x_\gamma + \delta_{\beta\gamma} x_\alpha x_\mu + \delta_{\alpha\gamma} x_\beta x_\mu)] \quad (13)$$

where the derivative is with respect to  $r = |\mathbf{r}|$  and  $x_\alpha$  is the  $\alpha$ th component of  $\mathbf{r}$ . The sum runs over all pairs of particles separated by the vector  $\mathbf{r}$ , where one or both are inside a given coarse-graining box of volume  $V_c$ .  $r_{in}$  is the proportion of  $\mathbf{r}$  which lies inside the volume. Switching to the Voigt notation  $C_{ij}^V = C_{\alpha\beta\gamma\mu}$  ( $xx = 1, yy = 2, zz = 3, yz = 4, xz = 5, xy = 6$ ) the Kelvin matrix  $C_{ij}$  is defined by  $C_{ij} = C_{ij}^V$ ,  $i, j \leq 3$ ;  $C_{ij} = 2C_{ij}^V$ ,  $i, j \geq 4$ ;  $C_{ij} = \sqrt{2}C_{ij}^V$ ,  $i \leq 3, j \geq 4$  or  $i \geq 4, j \leq 3$ . For an isotropic system the 6 eigenvalues of  $C_{ij}$  are  $3K$  (non-degenerate) and  $2G$  (five-fold degenerate)<sup>33,36</sup>.

1. Elliott, S. R. *Physics of amorphous materials* (Wiley, New York, 1984).
2. Kob, W. & Binder, K. *Glassy Materials and Disordered Solids: An Introduction* (World Scientific, London, 2011).
3. Maradudin, A. A. *Lattice dynamics* (Benjamin, New York, 1969).
4. Buchenau, U., Nücker, N. & Dianoux, A. J. Neutron scattering study of the low-frequency vibrations in vitreous silica. *Phys. Rev. Lett.* **53**, 2316–2319 (1984).
5. Monaco, G. & Giordano, V. M. Breakdown of the debye approximation for the acoustic modes with nanometric wavelengths in glasses. *PNAS* **106**, 3659–3663 (2009).
6. Baldi, G., Giordano, V. M., Monaco, G. & Ruta, B. Sound attenuation at terahertz frequencies and the boson peak of vitreous silica. *Phys. Rev. Lett.* **104**, 195501 (2010).
7. Ruta, B. *et al.* Communication: High-frequency acoustic excitations and boson peak in glasses: A study of their temperature dependence. *The Journal of Chemical Physics* **133**, 041101 (2010).
8. Baldi, G., Giordano, V. M. & Monaco, G. Elastic anomalies at terahertz frequencies and excess density of vibrational states in silica glass. *Phys. Rev. B* **83**, 174203 (2011).



9. Zeller, R. C. & Pohl, R. O. Thermal conductivity and specific heat of noncrystalline solids. *Phys. Rev. B* **4**, 2029–2041 (1971).
10. Alexander, S., Entin-Wohlman, O. & Orbach, R. Phonon-fracton anharmonic interactions: The thermal conductivity of amorphous materials. *Phys. Rev. B* **34**, 2726–2734 (1986).
11. Schirmacher, W. Thermal conductivity of glassy materials and the boson peak” *Europhys. Lett.* **73**, 892–898 (2006).
12. Schmid, B. & Schirmacher, W. Raman scattering and the low-frequency vibrational spectrum of glasses. *Phys. Rev. Lett.* **100**, 137402–(4) (2008).
13. Unruh, T., Schulte, A., Guo, Y., Schirmacher, W. & Schmid, B. Inelastic neutron and low-frequency raman scattering in a niobium-phosphate glass for raman gain applications. *J. Non-Cryst. Sol.* **357**, 506–509 (2011).
14. Schulte, A., Schirmacher, W., Schmid, B. & Unruh, T. Inelastic neutron and low-frequency raman scattering in niobium-phosphate glasses: the role of spatially fluctuating elastic and elasto-optic constants. *J. Phys. Condens. Matter* **23**, 254212–(25) (2011).
15. Zorn, R. The boson peak demystified? *Physics* **4**, 44–45 (2011).
16. Buchenau, U., Galperin, Y. M., Gurevich, V. L. & Schober, H. R. Anharmonic potentials and vibrational localization in glasses. *Phys. Rev. B* **43**, 5039–5045 (1991).
17. Gurevich, V. L. & Schober, H. R. Decay of mesoscopically localized vibrational eigenstates in porous materials. *Phys. Rev. B* **57**, 11295–11302 (1998).
18. Gurevich, V. L., Parshin, D. A. & Schober, H. R. Anharmonicity, vibrational instability, and the boson peak in glasses. *Phys. Rev. B* **67**, 094203–(10) (2003).
19. Duval, E., Mermet, A. & Saviot, L. Boson peak and hybridization of acoustic modes with vibrations of nanometric heterogeneities in glasses. *Phys. Rev. B* **75**, 024201–(9) (2007).
20. Schirmacher, W., Diezemann, G. & Ganter, C. Harmonic vibrational excitations in disordered solids and the “boson peak”. *Phys. Rev. Lett.* **81**, 136–139 (1998).
21. Götz, W. & Mayr, M. R. Evolution of vibrational excitations in glassy systems. *Phys. Rev. E* **61**, 587–606 (2000).
22. Kantelhardt, J. W., Russ, S. & Bunde, A. Excess modes in the vibrational spectrum of disordered systems and the boson peak. *Phys. Rev. B* **63**, 064302–(4) (2001).
23. Schirmacher, W., Ruocco, G. & Scopigno, T. Acoustic attenuation in glasses and its relation with the boson peak. *Phys. Rev. Lett.* **98**, 025501–(4) (2007).
24. Taraskin, S. N., Loh, Y. L., Natarajan, G. & Elliott, S. R. Origin of the boson peak in systems with lattice disorder. *Phys. Rev. Lett.* **86**, 1255–1258 (2001).
25. Chumakov, A. I. *et al.* Equivalence of the boson peak in glasses to the transverse acoustic van hove singularity in crystals. *Phys. Rev. Lett.* **106**, 225501–(5) (2011).
26. Bove, L. E. *et al.* Brillouin neutron scattering of -. *Europhys. Lett.* **71**, 563–569 (2005).
27. Caponi, S. *et al.* Raman-scattering measurements of the vibrational density of states of a reactive mixture during polymerization: Effect on the boson peak. *Phys. Rev. Lett.* **102**, 027402–(4) (2009).
28. Horbach, J., Kob, W. & Binder, K. High frequency sound and the boson peak in amorphous silica. *Eur. Phys. J. B* **19**, 531–543 (2001).
29. Schober, H. R. Vibrations and relaxations in a soft sphere glass: boson peak and structure factors. *J. Phys. Condens. Matter* **16**, S2659–S2670 (2004).
30. Pilla, O. *et al.* The low energy excess of vibrational states in  $v - sio_2$ : the role of transverse dynamics. *J. Phys. Condens. Matter* **16**, 8519–8530 (2004).
31. Leonforte, F., Boissière, R., Tanguy, A., Wittmer, J. P. & Barrat, J.-L. Continuum limit of amorphous elastic bodies. iii. three-dimensional systems. *Phys. Rev. B* **72**, 224206–(11) (2005).
32. Léonforte, F., Tanguy, A., Wittmer, J. P. & Barrat, J.-L. Inhomogeneous elastic response of silica glass. *Phys. Rev. Lett.* **97**, 055501–(4) (2006).
33. Mayr, S. G. Relaxation kinetics and mechanical stability of metallic glasses and supercooled melts. *Phys. Rev. B* **79**, 060201–(4) (2009).
34. Shintani, H. & Tanaka, H. Universal link between the boson peak and transverse phonons in glass. *Nature Materials* **7**, 870–877 (2008).
35. Monaco, G. & Mossa, S. Anomalous properties of the acoustic excitations in glasses on the mesoscopic length scale. *PNAS* **106**, 16907–16912 (2009).
36. Derlet, P. M., Maass, R. & Löffler, J. F. The boson peak of model galss systems and its relation to atomic structure. *Eur. Phys. J. B* **85**, 148–168 (2012).
37. Scopigno, T., Suck, J.-B., Angelini, R., Albergamo, F. & Ruocco, G. High-frequency dynamics in metallic glasses. *Phys. Rev. Lett.* **96**, 135501–(4) (2006).
38. Rufflé, B., Guimbretière, G., Courtens, E., Vacher, R. & Monaco, G. Glass-specific behavior in the damping of acousticlike vibrations. *Phys. Rev. Lett.* **96**, 045502–(4) (2006).
39. Srolovitz, D., Maeda, K., Vitek, V. & Egami, T. Structural defects in amorphous solids statistical analysis of a computer model. *Philos. Mag. A* **44**, 847–866 (1981).
40. Egami, T. & Srolovitz, D. Local structural fluctuations in amorphous and liquid metals: a simple theory of the glass transition. *J. Phys. F: Metal Physics* **12**, 2141–2163 (1982).
41. Duval, E., Boukenter, A. & Achibat, T. Vibrational dynamics and the structure of glasses. *J. Phys. Condens. Matter* **2**, 10227–10234 (1990).
42. Russell, E. V. & Israeloff, N. E. Direct observation of molecular cooperativity near the glass transition. *Nature* **408**, 695–698 (2000).
43. Wagner, H. *et al.* Local elastic properties of a metallic glass. *Nature Materials* **10**, 439–442 (2011).
44. Luchnikov, V. A., Medvedev, N. N., Naberukhin, Y. I. & Novikov, V. N. Inhomogeneity of the spatial distribution of vibrational modes in a computer model of amorphous argon. *Phys. Rev. B* **51**, 15569–15572 (1995).
45. Vollmayr-Lee, K., Kob, W., Binder, K. & Zippelius, A. Dynamical heterogeneities below the glass transition. *J. Chem. Phys.* **116–125**, 5158 (2002).
46. Tsamados, M., Tanguy, A., Goldenberg, C. & Barrat, J.-L. Local elasticity map and plasticity in a model lennard-jones glass. *Phys. Rev. E* **80**, 026112–(17) (2009).
47. Rahman, A., Mandell, M. J. & McTague, J. P. Molecular dynamics study of an amorphous lennardjones system at low temperature. *J. Chem. Phys.* **64–69**, 1564 (1976).
48. Strutt, J. W. (Lord Rayleigh) On the transmission of light through an atmosphere containing small particles in suspension, and on the origin of the blue of the sky. *Philos. Magazine* **47**, 375–384 (1903).
49. Jackson, J. D. *Classical Electrodynamics* (Wiley, New York, 1975).
50. Klemens, P. G. The thermal conductivity of dielectric solids at low temperatures. *Proc. Phys. Soc. London, Ser.* **208**, 108–133 (1951).
51. Akkermans, E. & Maynard, R. Weak localization and anharmonicity of phonons. *Phys. Rev. B* **32**, 7850–7862 (1985).
52. Elliott, S. R. A unified model for the low-energy vibrational behaviour of amorphous solids. *Europhys. Lett.* **19**, 201–206 (1992).
53. Ganter, C. & Schirmacher, W. Rayleigh scattering, long-time tails, and the harmonic spectrum of topologically disordered systems. *Phys. Rev. B* **82**, 094205–(7) (2010).
54. Zanatta, M. *et al.* Debye to non-debye scaling of the boson peak dynamics: Critical behavior and local disorder in vitreous germania. *J. Chem. Phys.* **135**, 174506–(5) (2011).
55. Beltukov, Y. M. & Parshin, D. A. Theory of sparse random matrices and vibrational spectra of amorphous solids. *Physics of the Solid State* **53**, 151–162 (2011).
56. Köhler, S. *Diploma thesis* (Univ. Mainz, unpublished, 2011).
57. Kob, W. & Andersen, H. C. Scaling behavior in the  $\beta$ -relaxation regime of a supercooled lennard-jones mixture. *Phys. Rev. Lett.* **73**, 1376–1379 (1994).
58. Allsopp, N., Ruocco, G. & Fratolocchi, A. Molecular dynamics beyonds the limits: Massive scaling on 72 racks of a bluegene/p and supercooled glass dynamics of a 1 billion particles system. *Journal of Computational Physics* **231**, 3432 – 3445 (2012).
59. Ashcroft, N. W. & Mermin, N. D. *Solid State Physics* (Holt, Rinehart, Winston, New York, 1976).

## Acknowledgement

W. S. is grateful for helpful discussions with J.-L. Barrat and H. R. Schober. For parallel computing, this research used the resources of the Supercomputing Laboratory and the Primalight group at KAUST University.

## Author contributions

A.M., A.F., W.S. and G.R. work at the simulations and field theoretical analysis. A.M., A.F., W.S. and G.R. reviewed the manuscript.

## Additional information

**Competing financial interests:** The authors declare no competing financial interests.

**License:** This work is licensed under a Creative Commons

Attribution-NonCommercial-NoDerivs 3.0 Unported License. To view a copy of this license, visit <http://creativecommons.org/licenses/by-nc-nd/3.0/>

**How to cite this article:** Marruzzo, A., Schirmacher, W., Fratolocchi, A. & Ruocco, G. Heterogeneous shear elasticity of glasses: the origin of the boson peak. *Sci. Rep.* **3**, 1407; DOI:10.1038/srep01407 (2013).